American Mineralogist, Volume 70, pages 149–158, 1985

Existence of multiple kaolinite phases and their relationship to disorder in kaolin minerals

STEPHAN DELUCA AND M. SLAUGHTER

Department of Chemistry and Geochemistry
Colorado School of Mines, Golden, Colorado 80401

Abstract

Previous research describing kaolinite X-ray diffraction patterns predicted that disorders in the crystal structure cause the observed deformations of diffraction profiles. Although disorders, such as $\pm b/3$ layer translations and random aluminum vacancies explain many of the profile shapes, they do not contribute to asymmetry in $00l$ profiles or the appearance of "anomalous" peaks in some diffraction patterns of poorly crystallized kaolinites.

The disparity in measured values of kaolinite physical properties, e.g., unit cell dimensions, differential thermal analysis and infrared spectra, and free energy of formation, indicate the possible existence of multiple kaolinite phases. The presence of multiple phases is (theoretically) shown to cause certain observed diffraction effects that are not explained by random disorders. The use of a deconvolution technique to obtain X-ray diffraction profiles, free of instrumental aberration, confirms the presence of multiple, well-crystallized kaolinite phases in a sample of Keokuk, Iowa geode-kaolinite. Diffraction patterns of ground samples of Keokuk kaolinite indicate that phase changes, as well as $\pm b/3$ layer shifts, occur with grinding. The existence of multiple, well-crystallized kaolinite phases may account for the physical properties of kaolinites as much as the sample's degree of crystallinity.

Introduction

Interpretations of kaolinite X-ray diffraction patterns (Brindley and Robinson, 1946; Murray and Lyons, 1956, Newnham, 1961) suggested that layer shifts occur along the **b** axis with displacements nearly equal to $\pm nb/3$. The number of shifted layers determined the mineral's crystallinity.

The kaolin minerals, in general, exhibit $\pm nb/3$ shifts as evidenced by their X-ray powder patterns. Grim (1968) shows how the powder diagrams change with the degree of kaolinite crystallinity. The reflections with a k-index equal to 3n (n = 1,2 . . . .) are largely unaffected. Those with $b \neq 3n$ broaden asymmetrically, become weaker or disappear as the crystallinity decreases. Inspection of the kaolin diffractograms reveals a change in the shape, intensity, and position of the $00l$ profiles (Mitra, 1963), evidence that changes in the interlayer spacing accompany stacking faults. For extreme disorder, the reflections with $b = 3n$ also broaden and deform, showing that structural models which contain only $nb/3$ translations of random layers, or random aluminum vacancies cannot explain the powder X-ray diffractograms.

Plancon and Tchoubar (1977a,b) proposed a model in which random aluminum vacancies accompany random layer translations. They integrated the works of Hendrix and Teller (1942), Mering (1949), Wilson (1949a,b) and Brindley and Mering (1948) to calculate theoretical diffraction profiles for a structure with a given proportion of each type of defect. The structural model which produces the closest match between theoretical and observed profiles is assumed to be the real crystal structure. The method of Plancon and Tchoubar produces profiles that fit well for certain samples. They did not study asymmetric broadening of the $(00l)$ profiles, but rather assumed a constant basal spacing for determination of the number of layers. Their method, of course, does not account for the appearance of "anomalous" peaks in some kaolinite diffraction patterns.

Although the Plancon and Tchoubar method addresses random disorders very well, anomalous kaolinite diffraction profiles lead to the hypothesis that some of the diffraction properties associated with disorder in kaolinite result from the creation or presence of multiple, at least moderately well-crystallized, phases. Indeed, multiple crystalline kaolinite phases might explain asymmetric $00l$ profiles, deformations in the $k = 3n$ hkl profiles and the appearance of seemingly anomalous peaks in some diffraction patterns.

There is indirect evidence for multiple kaolinite phases. Unit cell dimensions for kaolinite have been determined by X-ray powder and single crystal diffraction as well as electron diffraction studies (Brindley and Robinson, 1946; Drits and Kashaev, 1960; Zvyagin, 1967), each study

0003–004X/85/0102–0149$02.00

giving different unit cells. Dehydroxylation temperatures, infrared absorption spectra, and experimentally determined free energies of formation of kaolinite vary significantly. Keller and Haenni (1978) suggest that the disparate kaolinite free energies of formation may be due to non-monomineralic samples, although they do not imply multiple kaolinite phases.

Radoslovich (1963), observed that (1) the Si–O and O–H–O bonds are not very compliant; (2) the O–H bonds are strongly directed, at an inclined angle to c*; and (3) the O–Si–O angles are quite compliant, and concluded that interlayer hydrogen bonding acts to reduce the size of the tetrahedral base triads. These observations suggest that a change in the intralayer configuration may accompany a relative shifting of layers, even though the interlayer hydrogen bonds are much weaker than the intralayer bonds.

The purpose of this study was to investigate three hypotheses for the cause of the diffraction profiles in "disordered" kaolinites: (1) diffraction profiles broaden and become asymmetric with $\pm nb/3$ shifts; (2) multiple, well-crystallized phases cause the broadening and asymmetry; and (3) both hypotheses (1) and (2) contribute to the diffraction profiles. Diffraction patterns of pristine and ground samples of the well-crystallized Keokuk kaolinite (Keller et al., 1966, Keller and Haenni, 1978) were analyzed to test the hypotheses. We briefly summarize the contributions of stacking faults, multiple phases, systematic errors in X-ray profiles and the deconvolution to remove systematic error and improve resolution of severely overlapped kaolinite profiles. Finally, X-ray diffraction results are presented and interpreted through random defect and multiple phase models.

Theory

Representing each atomic position in a crystal is a vector R_n from an arbitrary origin to the atom's position in the unit cell (r_n) and the position of the unit cell in the crystal,

$$R_n = r_n + m_1 a + m_2 b + m_3 c. \tag{1}$$

a, b, and c are the unit cell vectors and m_1, m_2, m_3 are integers. The intensity of diffraction is (Warren, 1969)

$$I = I_e |F|^2 \frac{\sin^2 S\, M_1 a \cdot \sin^2 S\, M_2 b \cdot \sin^2 S\, M_3 c}{\sin^2 S\, a \cdot \sin^2 S\, b \cdot \sin^2 S\, c}, \tag{2}$$

where $I_e = e^4 I_o(1+\cos 2\theta)/2m^2c^2R^2$, I_o is the intensity of the incident non-polarized X-ray beam, F is the structure factor, S is the reciprocal vector, and M is the number of atoms in the a, b, or c directions. A diffraction profile is then symmetrical except for the effect of the polarization term in I_e and is symmetrical even if M is small (small particle size).

When stacking faults occur, the vector R_n, describing each atomic position, is redefined in terms of layer shifts with respect to an arbitrary origin, i.e., δ along $\hat{a}$ and ϵ along $\hat{b}$:

$$R_m^n = r_n + m_1\hat{a} + m_2\hat{b} + \gamma_{m3} + \delta_{m3}\hat{a} + \epsilon_{m3}\hat{b}, \tag{3}$$

where $|\gamma_{m3}|$ is the perpendicular distance to the m_3 layer. The intensity function reduces to

$$I = |F|^2 \frac{\sin^2\pi h M_1 \cdot \sin^2\pi k M_2}{\sin^2\pi h \cdot \sin^2\pi k} \sum_{m_3} \sum_{m_3'} \exp - 2i[S \cdot (\gamma_{m3} - \gamma_{m3'}) + (\delta_{m3} - \delta_{m3'})h + (\epsilon_{m3} - \epsilon_{m3'})k] \tag{4}$$

For $00l$ reflections the exponential term in the summation is $\exp^{-2iS\cdot(\gamma_{m3}-\gamma_{m3'})}$.

For a kaolinite having random layers translated by $\pm nb/3$, the $00l$ and hkl ($k = 3n$) reciprocal lattice consists of discrete points, whereas the hkl ($k \neq 3n$) reciprocal lattice consists of rods extending parallel to c*. Both the reciprocal lattice points and rods have some thickness. Thus, the intensity distributions for $00l$ and $k = 3n$ reflections are "normal", i.e., the same as those for an unfaulted (mosaic) sample. The $k \neq 3n$ profiles do not fit normal analytical functions, instead they rise sharply on the low 2θ angle side and tail off on the high angle side. The profile maxima occur at the same angle as in a sample containing mosaic crystals.

Although equation (4) would give symmetric $00l$ profiles for kaolinite with stacking faults, if faulting results in a change in $d(00l)$, asymmetry in these reflections ensues. Introducing the probability function P(Δ), the probability that a certain interlayer distance Δ exists in the crystal, the summations of (4) become

$$N \int P(\Delta) e^{-2i\Delta S} d\Delta \tag{5}$$

where N is the number of layers minus one. Expression (5) is the Fourier transform p(S) of the distribution of interlayer spacings P(Δ) (MacEwan, 1956).

The contribution of expression (5) to the diffraction profile shape depends on the distribution of spacings about the most probable spacing. An asymmetric distribution of spacings produces an asymmetric profile. However, expression (5) would also apply when multiple phases are present. If two kaolinite phases with distinct $00l$ spacings are present together, the population of spacing of both phases results in a bimodal P(Δ) and therefore an asymmetric or bimodal diffraction profile. Thus, asymmetric $00l$ P(Δ) in kaolinite may be caused by (1) the presence of multiple phases with similar d-spacings, or (2) a single disordered phase in which layer translations are accompanied by a change in interlayer distance. The phase and stacking fault models predict a shift of $00l$ peak positions as the phase populations change.

To interpret the powder diffraction profiles of kaolinite, abberations must be removed. The intensity expressions including particle size broadening, stacking fault broadening and asymmetry give profiles which we shall call the "pure" profiles. The Lorentz-polarization term, wavelength dispersion, slit effects, etc., cause broadening and asymmetric aberrations of pure diffraction profiles. Several authors (Patterson, 1950; Porteus, 1961; Sauder, 1966; Mitchell and deWolff, 1967; Ergun, 1968; Taupin, 1973; Parrish, et al., 1976; Huang and Parrish, 1977, Slaughter, 1981) describe convolution functions to remove instrumental and other aberrations from observed X-ray diffraction profiles.

For X-ray diffraction profiles, the observed intensity, h(ϵ) is given by

$$h(\epsilon) = \int p(\epsilon') q(\epsilon - \epsilon') d\epsilon'. \tag{6}$$

Equation (6) may be represented as h(ϵ) = p*q, where the *

indicates convolution. For n factors contributing to the observed profile, including the pure profile

$$h(\epsilon) = f_1(\epsilon_1)*f_2(\epsilon_2)* \ldots *f_n(\epsilon_n)+b(\epsilon), \quad (7)$$

where $b(\epsilon)$ is the background intensity. Grouping the terms of crystal effects (pure profile) into a function f and grouping geometrical, wavelength and instrumental abberations into a function g, the observed intensity profile results from folding these two functions and adding the background:

$$h(\epsilon) = f*g + b. \quad (8)$$

If g or f is known (numerically) over a 2θ interval, an unfolding process (deconvolution) determines the other (Ergun, 1968).

Experimental

Sample processing and X-ray analysis

A pure, well-crystallized sample of kaolinite was selected for this study. Dr. W. D. Keller provided Keokuk-geode kaolinite, which is reported to be the best crystallized kaolinite yet found (Keller, 1977), and was therefore thought suited for use as a standard material.

The kaolinite was shaken by hand from its containing geode, sieved to less than 150 mesh, mixed, split into three portions, then processed as follows: (1) untreated (standard sample); (2) hand ground for two minutes (2 min-grind) with a miniature jade mortar and pestle; and (3) hand ground for three minutes (3 min-grind). Grinding is known to change kaolinite diffraction patterns. These changes have been interpreted as being due to a decrease in the crystallinity (an increase in the number of stacking faults) of the sample with grinding. The ground samples were used to determine if grinding causes stacking faults, phase changes or a combination of the two.

Each of the three samples was sieved, through a 150 mesh sieve, into X-ray diffraction sample holders. A glass slide was placed over the holder to level the sample with the face of the sample holder. Portions of the standard and 2 min-grind samples were also sieved onto scanning electron microscope (SEM) sample holders, and coated with gold for SEM viewing.

Fast-scanned X-ray powder diffraction patterns for the standard and 2 min-grind samples were obtained with an automated, wide-angle Philips vertical diffractometer, using copper radiation, a crystal monochromator and a scintillation detector. Scans from 2° to 60° 2θ were recorded on strip charts for the standard and ground samples, with a scan speed of ½° 2θ per minute at 1000 counts full scale.

Step scans were taken for several $\Delta\ 2\theta$ ranges at 0.02° per step with 30 second counting times for the standard and 2 min-grind samples. Digital intensities were recorded as counts per step by an interfaced Honeywell H316 computer, and analog intensities were recorded on the strip-chart recorder.

The diffraction patterns for the 3 min-grind sample and duplicate patterns for several standard and 2 min-grind samples were collected with a manual narrow-angle Philips vertical diffractometer using a scintillation counter, without monochromator. The scans were manually stepped at 0.02° intervals with 20 second counting times.

The standard sample was observed with a JEOL scanning electron microscope at Marathon Oil Company's Denver Research Center. The standard and 2 min-grind samples were observed on the Colorado School of Mines Crystal Research Laboratory's JEOL scanning electron microscope. These observations showed that the kaolinite particles are platy, and range from 1 μm to 10 μm in the **a** and **b** crystallographic directions (parallel to the plates), and from 2 μm to less than 1 μm in the **c**-direction. No significant changes in either morphology or particle size were observed in the ground sample relative to the standard sample.

Profile correction

The program ISTRIP (Slaughter, 1981) corrected the diffraction profiles to obtain pure crystalline profiles. Calculations were done on the CSM DEC System 10 computer. ISTRIP uses Ergun's (1968) method to remove intensity contributions due to all but the crystalline (including defect structure) effects. In the Ergun method either function g or h may be unbounded, but better convergence resulted when g was unbounded. It was found essential that the function used to determine g has smooth background on both sides. Background statistical errors do not necessarily give poor Ergun method convergence, but spurious peaks due to background errors show in final f-profiles.

The sequence for determining corrected profiles (f's) is as follows:

(1) The $K\alpha_1$ profile of a pure quartz standard at a high angle (90.6° 2θ) is used to calculate a Lorentzian curve corresponding to the "pure" profile.

(2) The Lorentzian profile from (1) is deconvoluted from the observed profile of a standard mineral (e.g., quartz and gypsum). The resulting profile becomes the g-function for any kaolinite reflections near it.

(3) The g-function is tested by deconvoluting it from the observed standard profile. A correct g-function produces a Lorentzian curve similar to that calculated in step 1.

(4) The g-function is deconvoluted from the kaolinite profile producing the corrected (crystalline) profile.

ISTRIP fits corrected profiles to sums of Lorentzians by a method of stripping followed by nonlinear least squares refinement. The fitted curves are actually sums of Lorentzians modified by a power parameter (Taupin, 1973). Each Lorentzian is of the form

$$f_m(x_i) = \frac{P_1}{(x_i - P_2)^{P_4} + P_3^{P_4}} \quad (9)$$

where x_i is the ith abscissa point from the origin of the interval, P_1 is the peak intensity, P_2 is the peak position, P_3 is the half-width at half-height, and P_4 is a variable power parameter.

The 7.57Å reflection of a standard gypsum sample was used to determine the g-function in the range of the kaolinite (001) reflection. A quartz standard 20.86° 2θ reflection determined the g-function for the kaolinite 002 and *hk*-band reflections.

Results

Fast-scanned diffraction patterns

Each of the peaks on the fast-scanned patterns was initially indexed as a kaolinite reflection (Fig. 1). Figures 1–3 show how the fast-scanned patterns changed with grinding. The fast-scanned patterns and the corrected step-scanned data resulted in several lines in each sample

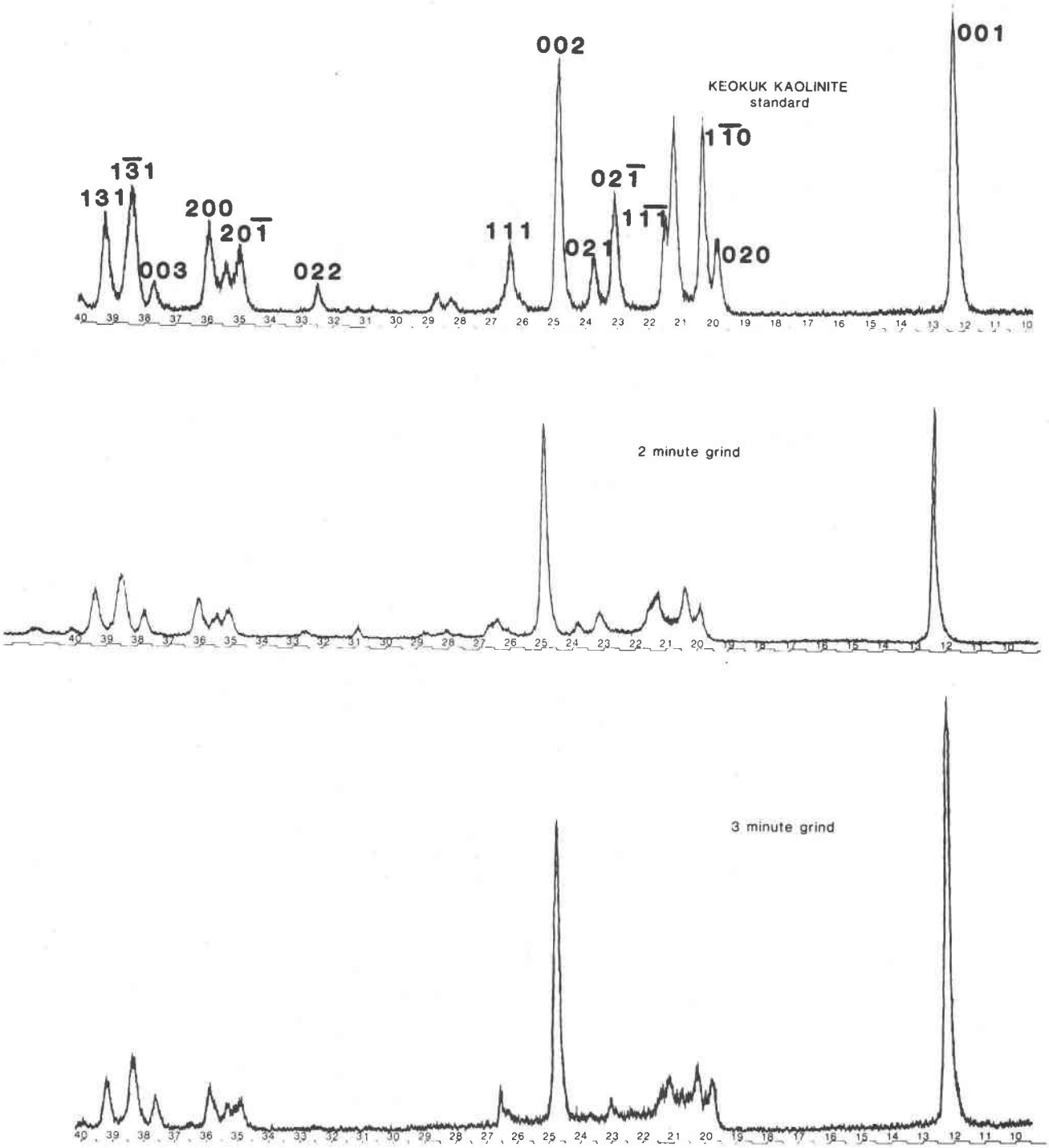

Fig. 1. Fast scanned diffraction patterns of Keokuk kaolinite showing indexing of peaks. The scale is in °2θ.

which could not be indexed as kaolinite or dickite reflections based on Newnham's unit cells.

The fast-scanned standard diffraction patterns look very similar to patterns published in previous works (Keller, 1978). The standard sample (Fig. 1) shows sharp, well-defined peaks even in the *hk*-zone (19°–24° 2θ). In the 2 min-grind pattern the *hk*-zone reflections are less intense than those of the standard and the (111) peak position is no longer determinable. This pattern resembles some of the "fairly well-crystallized" kaolinites such

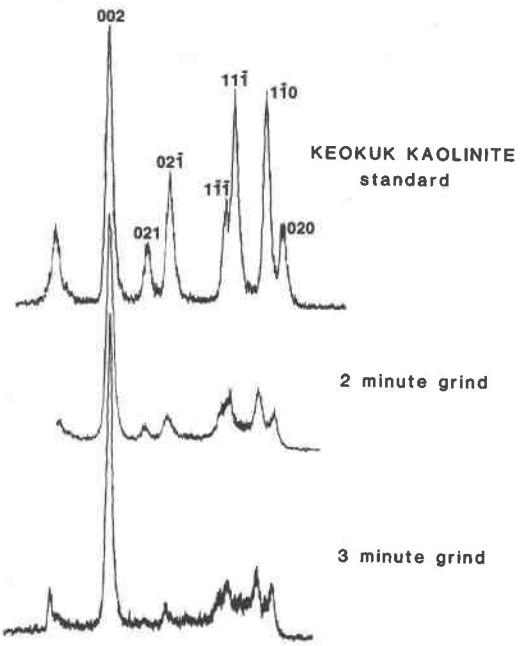

Fig. 2. Sequence showing effect of grinding on *kh*-band ($k \neq 3n$) of Keokuk kaolinite.

as the Murfreesboro kaolinite (Keller, 1978). The $k = 3n$ band (34°−40° 2θ) shows little change as would be expected for $\pm nb/3$ translational disorders.

The 3 min-grind pattern (Figs. 2, 3) does not conform to previously reported poorly-crystallized kaolinites. The *hk*-band shows a line between the 1$\bar{1}$0 and 11$\bar{1}$ and possibly the 020 and 1$\bar{1}$0 kaolinite reflections. Furthermore, the 1$\bar{1}$1 peak resolves from the 11$\bar{1}$ profile. The k = n profiles are broadened relative to the standard and 2 min-grind samples and an additional two peaks and a shoulder appear. The (new) peaks between 020 and 1$\bar{1}$0 and between 1$\bar{1}$0 and 11$\bar{1}$ do not index as kaolinite or dickite reflections (Table 1) based on the unit cell given by Newnham (1956).

Step-scanned profile patterns

Figures 4 and 5 illustrate the corrected and fitted profiles for the step-scanned 00*l* $\Delta 2\theta$ intervals. Figure 6 illustrates the corrected but not fitted profiles of the *hk*-band ($k \neq 3n$). Table 1 lists the calculated *d*-spacings for each fitted line. The angles at which the reflections occur do not necessarily give the true spacings. An internal standard was not used and different sample holders were used for each sample. The exact spacings would be useful for determining unit cell dimensions; however, findings of this study are not negated, since it is the difference in spacing between lines that is important.

The reproducibility of the fitted profiles was tested by running duplicate samples with the same diffraction conditions and also with different diffractometers and sample holders. Although profile intensities varied, the general features of the profiles were reproducible (Fig. 7).

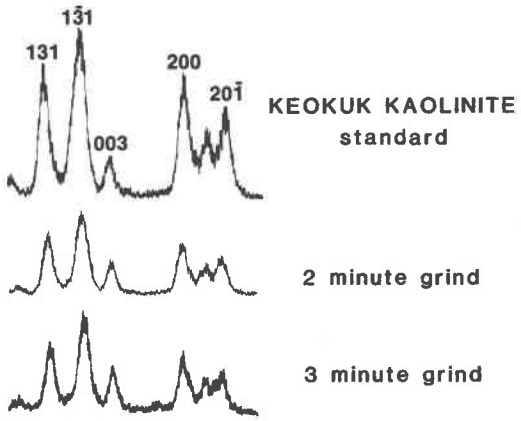

Fig. 3. Sequence showing effect of grinding on *hk*-band ($k = 3n$) of Keokuk kaolinite.

The Lorentzian-fitted 001 profiles of the three samples (Fig. 6) consist of two lines each: the most intense at about 7.14Å, and a low intensity line around 7.20Å. Grinding the sample causes the line at 7.20Å to increase relative to the 7.14Å line. The fast-scanned patterns do not resolve these lines.

The 002 profiles of the standard and 2 min-grind

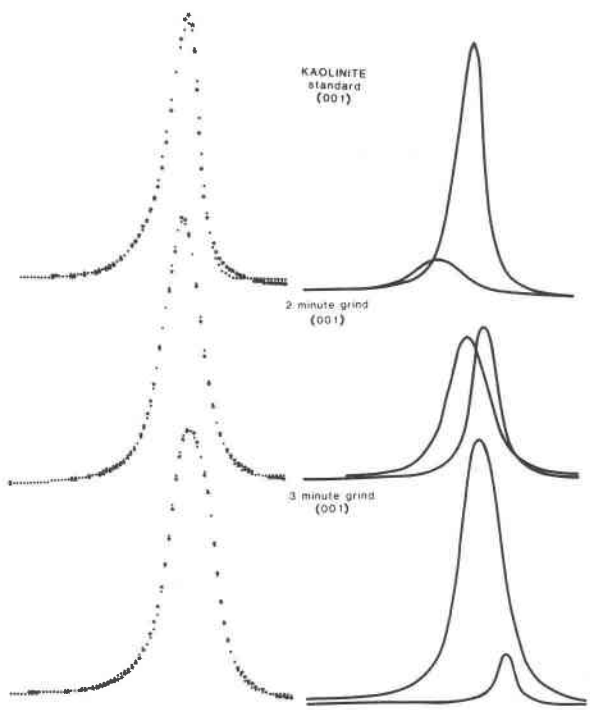

Fig. 4. Corrected and fitted profiles for Keokuk kaolinite 001 reflection. Denotes corrected experimental point, denotes fitted point, denotes coincident experimental and fitted point, denotes individual fitted curves. Angle increases to the right.

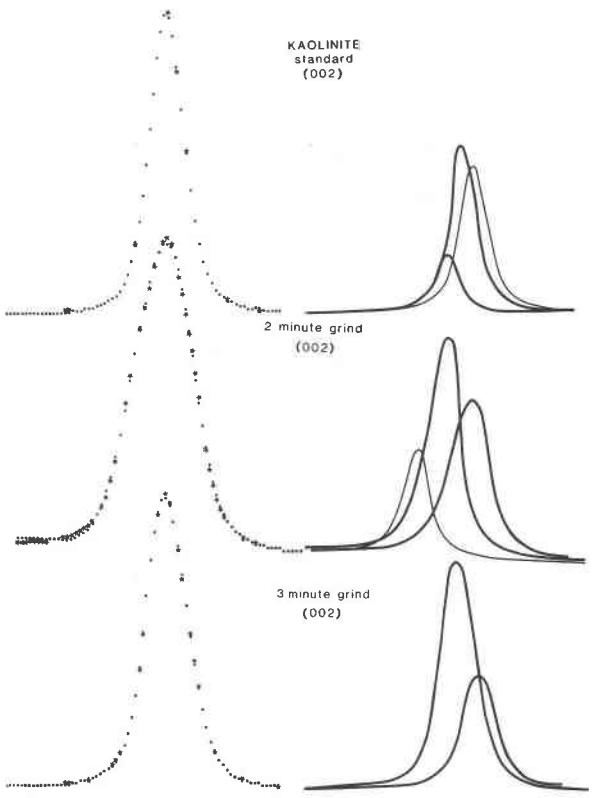

Fig. 5. Corrected and fitted profiles for Keokuk kaolinite 002 reflections.

Table 1. Corrected observed *d*-spacings for kaolinite reflections

Calculated (Newnham's Cell)	Observed Standard	Observed 2min-Grind	Observed 3min-Grind	hkl Index
7.12 Å	7.22 Å 7.14	7.19 Å 7.14	7.20 Å 7.14	001
3.56	3.57 3.58 3.60	3.57 3.58 3.60	3.57 3.59	002
4.46	4.47	4.46	4.46	020
4.35	4.37	4.36	4.36	$1\bar{1}0$
4.16	4.18	4.18	4.18	$11\bar{1}$
4.12	4.12	4.13	4.13	$\bar{1}\bar{1}1$

samples (Fig. 5) fit three lines: two lines of similar intensity at 3.56Å and 3.57Å, and a low intensity line (in the standard) at 3.60Å. The line at 3.56Å does not resolve in the 001 profiles. The 3.60Å line increases with grinding as does its corresponding (001) line. The 3.56Å line does not appear in the 3 min-grind sample.

Of importance is the transition from the standard to 3 min-grind sample in the *hk*-band (Fig. 6). The 2 min-grind profiles are broader and less resolved than the standard and 3 min-grind profiles. Also the (020) reflection in the 2 min-grind develops an inflection near the peak indicating the presence of two lines. A new line appears in the 3 min-grind sample at 4.25Å. This line causes the inflection between the $(1\bar{1}0)$ and $11\bar{1}$) in the 2 min-grind *hk*-band.

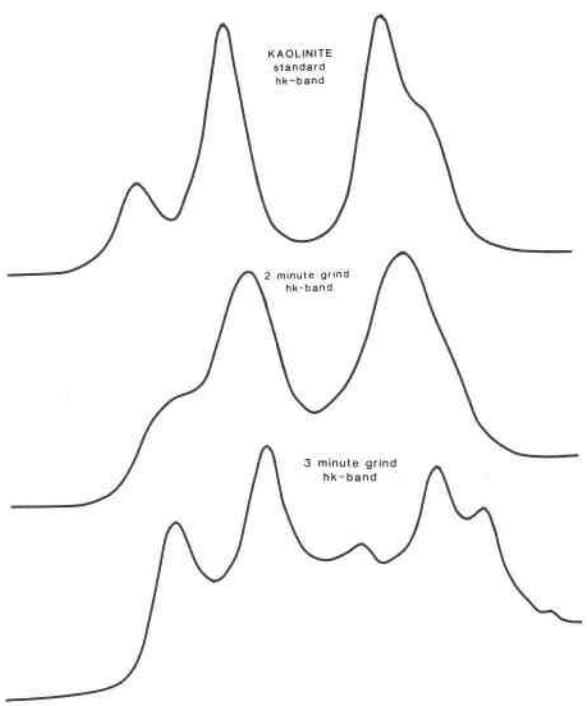

Fig. 6. Corrected *hk*-bands ($k \neq 3n$) for Keokuk kaolinite.

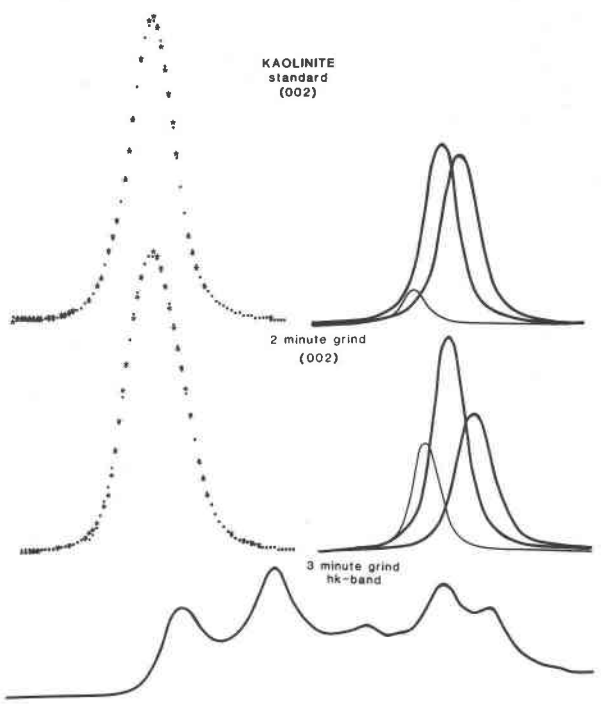

Fig. 7. Duplicate patterns for standard and 2-minute grind (002) profiles and 3 minute grind *hk*-band.

These effects are subtle, but noticeable in the fast-scanned patterns.

Interpretation of results

We must consider the validity of the fitted profiles. Do they correspond to discrete reflections or are they artifacts induced by deconvolution? Figures 8 and 9 present g-functions calculated for the quartz standard 20.9° 2θ reflection and the standard Keokuk kaolinite 002 reflection. These are the functions which, when convoluted with a Lorentzian, give the observed profiles. The quartz g-function shows two lines corresponding to reflections from $K\alpha_1$ and $K\alpha_2$ copper radiation. Deconvolution of the quartz g-function from the observed quartz profile gives a single Lorentzian. The kaolinite 002 profile produces a g-function containing three major lines. Instrumental and wavelength effects alone do not cause this pattern. The three lines correspond in relative intensity and position to the lines resolved by deconvolution of the quartz g-function from the observed standard 002 profile (Fig. 5). The three lines in the standard 002 profile correspond to three separate basal spacings. Deconvolution does not induce anomalous lines.

Several limitations complicate the interpretation of the *hk*-bands:

(1) A maximum of six lines could be fitted into each $\Delta 2\theta$ interval because of program constraints.

(2) The width of the high angle reflection used to calculate the g-function (e.g., quartz 90.5°) limits resolution of closely spaced lines. A higher angle line would have been preferable to further reduce aberrations in the data.

(3) Low peak-to-background ratios in the *hk*-band obscure low intensity profiles.

(4) The requirement of smooth background at the ends of the profile ranges prohibits analysis of each profile independently.

(5) Asymmetry due to stacking faults gives non-Lorentzian profiles.

For these reasons the *hk*-bands do not fit well with sums of Lorentzians as did the 00*l* profiles.

Even though Lorentzian fitting is poor, the corrected *hk*-band profiles reveal the phase changes shown in the 00*l* profiles. A line between $1\bar{1}0$ and $11\bar{1}$ appears in the Keokuk kaolinite *hk*-band with grinding. The line, which is incipient in the 2 min-grind pattern, becomes fully evident in the 3 min-grind pattern (Figs. 2 and 6). The line intensities coincide with the increasing 7.20Å phase; therefore, we attribute the 4.25Å reflection to the 7.20Å phase. The appearances of the line between the $1\bar{1}0$ and $11\bar{1}$ also coincides with the appearance of three lines in the *hk*-band (k = 3n) of Figure 3: between $13\bar{1}$ and $20\bar{1}$, between the 003 and 200, and a shoulder on the 200.

The 2 min-grind *hk*-band shows broadened profiles compared to the standard *hk*-band. The 020 and $1\bar{1}1$ lines are not as well defined in the 2 min-grind sample. This is consistent with a random disordering model requiring

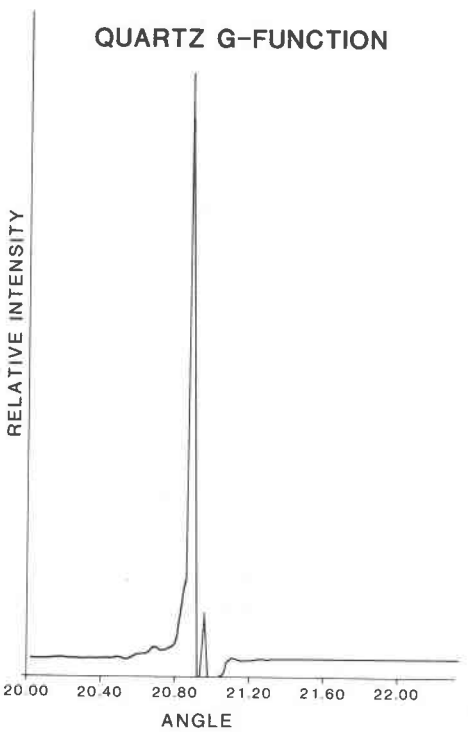

Fig. 8. Plot of the g-function calculated from the quartz 10.0° 2θ reflection. Angles are in °2θ.

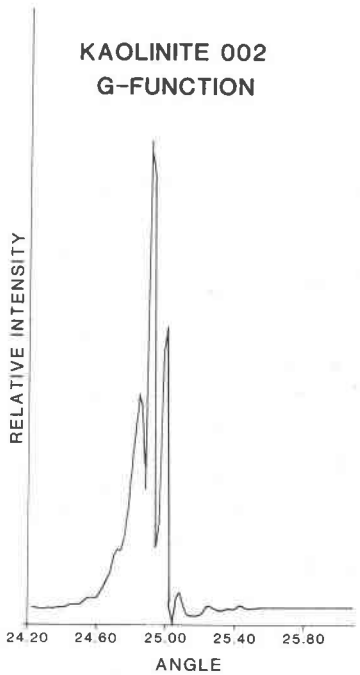

Fig. 9. Plot of the g-function calculated from the standard Keokuk kaolinite 002 reflection. Angles are in °2θ.

asymmetric broadening of profiles without shifting of modulation maxima.

The 001 profiles indicate two basal spacings: one at 7.14Å and the other at 7.20Å. The 7.14Å spacing is commonly reported for kaolinite. A 7.20Å spacing is usually only reported for poorly crystallized kaolinites (Grim, 1968). These spacings correspond to two separate phases in the Keokuk kaolinite. In the sequence from standard to 3 min-grind, the amount of 7.20Å phase increases at the expense of the 7.14Å phase. In the 3 min-grind sample the 7.20Å phase predominates.

Examining the consistency of the 002 with the 001 profiles, three peaks are present in the standard and 2 min-grind 002 profiles. The low-angle peak coincides with the 7.20Å 001 spacing. The middle peak is due to the 7.14Å phase. The third peak gives a basal spacing of 7.12Å, which is the spacing calculated for the unit cell by Newnham. The 7.12Å and 7.14Å phases do not resolve in the 001 profiles. The angular difference for 7.12Å and 7.14Å is only a few hundredths of a degree, which is below the resolution limits of the deconvolution.

As in the 001 profiles, the 002 profiles indicate an increasing 7.20Å phase relative to the 7.12Å and 7.14Å phases upon grinding. In the 3 min-grind sample the 7.12Å phase is destroyed.

It was previously thought that the sequence of kaolinite diffraction patterns from well-crystallized to "disordered" samples was caused by increasing amounts of random disordering in a single phase. These disorders include $\pm n b/3$ layer translations as well as random Al vacancies. Our results indicate that multiple well-crystallized kaolinite phases exist in the Keokuk geode-kaolinite. Furthermore, phase changes along with $\pm n b/3$ layer translations occur upon grinding the kaolinite.

Discussion

Comparison of results and predictions

Table 2 summarizes the relevant results and relates these observations to a model in which multiple crystalline phases, with concomitant random disordering, produce the observed sequence from standard to 3 min-grind samples. Random-defect-only models cannot account for observation 5; new lines are not produced by random disorders. Increasing disorder subdues modulations, so a defect model does not explain observation 6. Observations 1–3 require a change in the average basal spacing. Defects which occur as shifts only along *a* and/or *b* do not produce effects 1–3. Observation 4 is not explained by multiple well-crystallized phases.

Plancon and Tchoubar (1977b) noted that for their disordered kaolinites the 001 profile gave a 7.20Å basal spacing while the *hk*-band modulations indicated a 7.15Å spacing. Their interpretation is that the 00*l* and *hk* reflections diffract from different coherent volumes:

> "The coherent volume for the *hk*-band are the substackings limited by a random defect on each side; inside the substacking, the layers are equidistant as in the perfect triclinic kaolinite. On the contrary, the coherent volume producing the (00*l*) reflections includes the random defects; then a measurement, from the reflections, of a value of d_{001} greater than 7.15Å shows that the increase of basal distance is located only between two adjacent layers randomly translated."

Table 2. Interpretation of diffraction results

Observation	Implication
1) Calculation of a g-function with the standard (002) profile gives three lines.	At least three phases occur in Keokuk kaolinite (7.14Å, 7.12Å, 7.20Å).
2) Corrected (001) standard profile fits two lines. Corrected (002) standard profile fits three lines.	At least three phases occur. Two lines are too close to resolve in (001) profile.
3) Ground samples show sequential increase of the low angle lines in the (00ℓ) profiles with grinding.	7.20Å phase increases abundance relative to 7.12Å and 7.14Å phases.
4) 2min-grind hk-band gives broad unresolved profiles relative to standard hk-band; relative peak positions (020)(111) do not shift. k=3n profiles are not greatly affected.	Random layers shift $\pm n\underline{b}/3$ parallel to $\underline{ab}$ plane with grinding.
5) 2min-grind hk-band shows incipient line and 3min-grind hk-band shows resolved line between (110) and (11$\bar{1}$) reflections.	7.20Å phase is a crystalline phase and increases with grinding.
6) 3min-grind hk-band shows better resolution of lines than 2min-grind hk-band.	Disordered crystals shift to new phase (7.20Å).

Figure 4 shows a small peak occurring between the 1$\bar{1}$0 and 11$\bar{1}$ reflections. This peak cannot be accounted for, using only random defect models. The appearance of this line requires a multiple phase model to explain kaolinite diffraction patterns. The standard Keokuk kaolinite diffraction pattern fits the multiple-phase-only model. The ground sample patterns exhibit the effects of layer shifts, but also contain features which must be explained by the presence of multiple well-crystallized phases. We conclude that Keokuk kaolinite consists of several well- to moderately well-crystallized phases and that grinding the kaolinite induces phase conversions as well as random layer $\pm n b/3$ translations.

Association of phases with degree of crytallinity

The kaolinite unit cell, as given by Newnham (1956), predicts a basal spacing of 7.12Å. Resolution of the standard Keokuk kaolinite 002 profile produces a line corresponding to the 7.12Å phase. We interpret this phase as the ideal kaolinite. Disappearance of this phase in the 3 min-grind sample indicates that it exists as a major component only in very well-crystallized kaolinite samples.

Kaolinite diffraction data commonly report a 7.14Å spacing for well to reasonably-well-crystallized kaolinites. The 7.14Å phase persists in the ground samples.

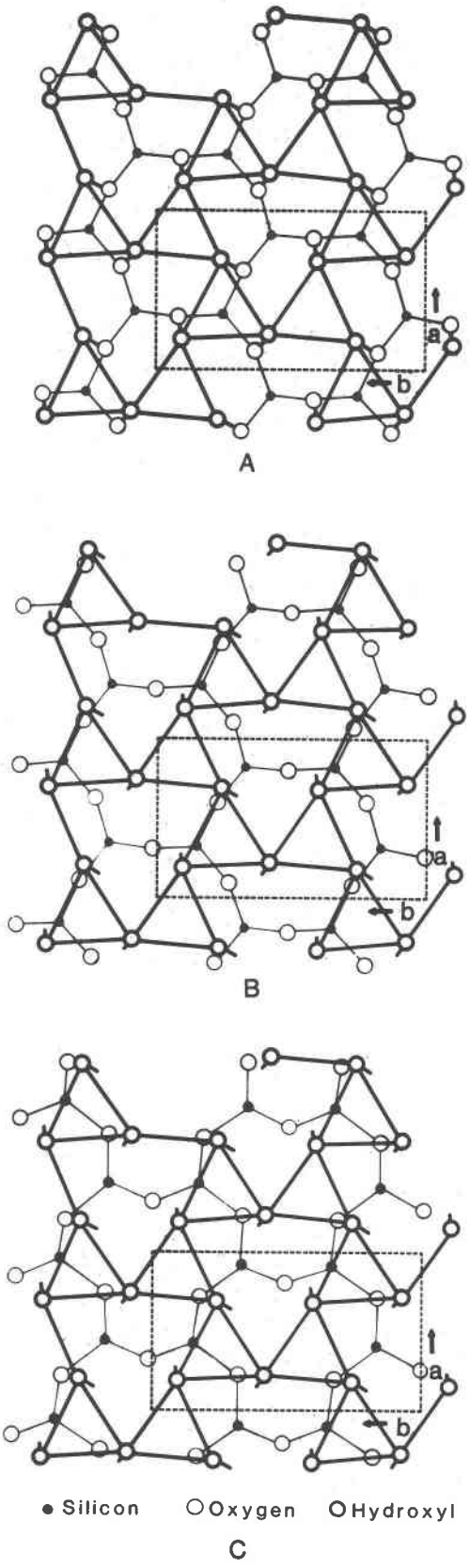

Random disorders occurring as $\pm nb/3$ shifts parallel to the *ab* plane in this phase cause broadening in the *hk*-band, but the modulation positions indicate that the intralayer structure remains constant, as do the α and β angles for substackings bounded by shifted layers.

Each of the three phases found in the Keokuk kaolinite associate with different degrees of total sample crystallinity. The 7.12Å phase associates with only well-crystallized samples, the 7.14Å phase with well to moderately-well-crystallized kaolinite, and the 7.20Å phase with poorly crytallized to extremely disordered samples. We do not imply that the 7.20Å phase is always largely disordered. On the contrary, at least a moderately well-crystallized 7.20Å phase exists, hence the line at 4.25Å. Other natural kaolinites may have three or more phases, some ordered and some disordered.

A model for kaolinite phase conversion

The association of the 7.20Å line with the appearance of a peak between the $1\bar{1}0$ and $11\bar{1}$ reflections requires for this possible new phase not only an increase in *c* but also an increase in α and/or β and possibly a decrease in the *a* and *b* dimensions relative to those of the 7.14Å phase. A qualitative model of the 7.20Å phase shows that a phase change from 7.14 to the 7.20Å phase is theoretically reasonable and consistent with the diffraction patterns:

(1) Grinding of ideal kaolinite induces layer shifts parallel to *b* which are *not* integral multiples of *b*/3 (Fig. 10B).

(2) These shifts decrease the stability of the interlayer hydrogen bonds.

(3) Decreased H-bond strength allows expansion of the basal spacing to reduce Si–Al, Si–Si and O–O repulsion.

(4) Oxygen tetrahedra counter-rotate (Fig. 10C) to increase H-bond strength (the surface OH positions are rigid, and counter-rotation of the tetrahedra occur even in the ideal kaolinite, partially to increase hydrogen bond strength (Radoslovich, 1963)).

Effects 2, 3 and 4 balance to give the final configuration of the 7.20Å phase, vis., increased *c* and α, and slightly decreased *a* and *b* relative to the ideal unit cell. An increase in α of only a few degrees with increase in *c* of about 0.1Å produces diffraction peaks in agreement with observed lines. This model is presented only to illustrate the *types* of changes which might occur to produce the observed diffraction effects.

Fig. 10. A. Interlayer bonding for a hypothetical kaolinite phase A. B. Interlayer bonding of kaolinite phase A after a relative shift along *b* less than *b*/3. Notice increased H-bond lengths. C. Interlayer bonding of kaolinite after tetrahedral base triads of a shifted layer rotate to increse H-bond strength (shorter bond lengths). These rotations may lead to a new metastable kaolinite phase B.

Acknowledgments

Thanks are extended to Mr. William Wiginton, at the Marathon Oil Research Center, Denver, for S.E.M. work, and to Dr. W. D. Keller, at the University of Missouri for providing a sample of Keokuk kaolinite.

References

Brindley, G. W. and Robinson, K. (1946) Randomness in the structures of kaolinitic clay minerals. Transactions of the Faraday Society, 42B, 198–205.

Brindley, G. W. and Mering, J. (1948) Banded X-ray Reflexions from Clay Minerals. Nature, 161, 774.

Drits and Kashaev (1960) Structural regularities of kaolinite minerals. Doklady Sobraniyu Mezhdunar, 15–18 (not seen; extracted from Zvyagin (1967)).

Ergun, S. (1968) Direct method for unfolding convolution products—its application to x-ray scattering intensities. Acta Crystallographica, 1, 19–23.

Grim, Ralph E. (1968) Clay Mineralogy, 2nd Edition. McGraw-Hill Book Company, New York.

Hendrix, S. and Teller, E. (1942) X-Ray interference in partially ordered layer lattices. Journal of Chemical Physics, 10, 147–167.

Huang, T. C. and Parish, W. (1977) Qualitative analysis of complicated mixtures by profile fitting x-ray diffractometer patterns. Advances in X-Ray Analysis, 19, 275–288.

Keller, W. D., Pickett, E. E. and Reesman, A. L. (1966) Elevated dehydroxylation temperature of the Keokuk geode kaolinite—A possible reference mineral. Proceedings of the International Clay Conference, Jerusaleum, 1, 75–85.

Keller, W. D. (1977) Kaolins collected from diverse environments of origin. Clays and Clay Minerals, 25(5), 341–345.

Keller, W. D. and Haenni, R. P. (1978) Effects of micro-sized mixtures of kaolin minerals on properties of kaolinites. Clays and Clay Minerals, 26(6), 384–396.

MacEwen, D. M. C. (1956) Fourier transform methods for studying scattering from lamellar systems. Kolloid-Zeitschrift, 149, 96–108.

Mering, J. (1949) L'Interference des rayons x dans les systemes a stratification Desordonnee. Acta Crystallographica, 2, 371–377.

Mitchell, C. M. and deWolff, D. (1967) Elimination of the dispersion effect in the analysis of diffraction line profiles. Acta Crystallographica, 22, 325–328.

Mitra, G. B. (1963) Structure defects in kaolinite. Zeitschrift für Kristallographie, 119, 161–175.

Murray, H. H. and Lyons, S. C. (1956) Correlation of paper-coating quality with degree of crystal perfection of kaolinite. Clays and Clay Minerals, 4, 31–40.

Newnham, R. E. (1956) Crystal structure of the mineral dickite. Ph.D. Thesis, The Pennsylvania State University.

Newnham, R. E. (1961) A refinement of the dickite structure and some remarks on polymorphism in kaolin minerals. Mineralogical Magazine, 32, 683–704.

Parrish, W., Huang, T. C. and Ayers, G. L. (1976) Profile Fitting: A powerful method of computer X-ray instrumentation and analysis. Transactions of the American Crystallographic Association, 12, 55–73.

Patterson, M. S. (1950) Calculation of the correction for instrumental broadening in x-ray diffraction lines. Proceedings of the Physical Society, London, A63, 477–482.

Plancon, A. and Tchoubar, C. (1977a) Determination of structural defects in phyllosilicates by X-ray powder diffraction—I. principal of calculation of the diffraction phenomenon. Clays and Clay Minerals, 25, 430–435.

Plancon, A. and Tchoubar, C. (1977b) Determination of structural defects in phyllosilicates by X-ray powder diffraction—II. nature and proportion of defects in natural kaolinites. Clays and Clay Minerals, 25, 436–450.

Porteus, J. O. (1961) Optimized method for correcting smearing abberations: complex X-ray spectra. Journal of Applied Physics, 33, 700–707.

Radoslovich, E. W. (1963) Layer lattice silicates. American Mineralogist, 48, 86–91.

Sauder, W. C. (1966) General method of treating instrumental distortion of spectral data with applications to x-ray physics. Journal of Applied Physics, 37, 1495–1507.

Slaughter, M. (1981) Deconvolution of overlapped X-ray powder diffraction spectra for quantitative analysis. In Electron Microscopy and X-Ray Applications to Environmental and Occupational Health Analysis, Volume 2, p. 77–114. Ann Arbor Science Publishers, Inc., Ann Arbor.

Taupin, D. (1973) Automatic peak determination in X-ray powder patterns. Journal of Applied Crystallography, 6, pp. 266–273.

Warren, B. E. (1969) X-Ray Diffraction. Addison-Wesley Publishing Company, Reading, Massachusetts.

Wilson, A. J. C. (1949a) X-ray diffraction by random layers: ideal line profiles and determination of structure amplitudes from observed line profiles. Acta Crystallographica, 2, 245–251.

Wilson, A. J. C. (1949b) The probability distribution of X-ray intensities. Acta Crystallographica, 2, 318–321.

Zvyagin, B. (1967) Electron-Diffraction Analysis of Clay Mineral Structures. Plenum Press, New York.

Manuscript received, March 10, 1983;
accepted for publication, July 30, 1984.